Lecture Notes in Mechanical Engineering

Volodymyr Tonkonogyi · Vitalii Ivanov · Justyna Trojanowska · Gennadii Oborskyi · Milan Edl · Ivan Kuric · Ivan Pavlenko · Predrag Dasic *Editors*

Advanced Manufacturing Processes

Selected Papers from the Grabchenko's International Conference on Advanced Manufacturing Processes (InterPartner-2019), September 10–13, 2019, Odessa, Ukraine

Springer

Lecture Notes in Mechanical Engineering (LNME) publishes the latest developments in Mechanical Engineering - quickly, informally and with high quality. Original research reported in proceedings and post-proceedings represents the core of LNME. Volumes published in LNME embrace all aspects, subfields and new challenges of mechanical engineering. Topics in the series include:

- Engineering Design
- Machinery and Machine Elements
- Mechanical Structures and Stress Analysis
- Automotive Engineering
- Engine Technology
- Aerospace Technology and Astronautics
- Nanotechnology and Microengineering
- Control, Robotics, Mechatronics
- MEMS
- Theoretical and Applied Mechanics
- Dynamical Systems, Control
- Fluid Mechanics
- Engineering Thermodynamics, Heat and Mass Transfer
- Manufacturing
- Precision Engineering, Instrumentation, Measurement
- Materials Engineering
- Tribology and Surface Technology

To submit a proposal or request further information, please contact the Springer Editor in your country:

China: Li Shen at li.shen@springer.com
India: Priya Vyas at priya.vyas@springer.com
Rest of Asia, Australia, New Zealand: Swati Meherishi at swati.meherishi@springer.com
All other countries: Dr. Leontina Di Cecco at Leontina.dicecco@springer.com

To submit a proposal for a monograph, please check our Springer Tracts in Mechanical Engineering at http://www.springer.com/series/11693 or contact Leontina.dicecco@springer.com

Indexed by SCOPUS. The books of the series are submitted for indexing to Web of Science.

More information about this series at http://www.springer.com/series/11236

Volodymyr Tonkonogyi · Vitalii Ivanov ·
Justyna Trojanowska · Gennadii Oborskyi ·
Milan Edl · Ivan Kuric · Ivan Pavlenko ·
Predrag Dasic
Editors

Advanced Manufacturing Processes

Selected Papers from the Grabchenko's International Conference on Advanced Manufacturing Processes (InterPartner-2019), September 10–13, 2019, Odessa, Ukraine

Springer

Editors
Volodymyr Tonkonogyi
Odessa National Polytechnic University
Odessa, Ukraine

Vitalii Ivanov
Sumy State University
Sumy, Ukraine

Justyna Trojanowska
Poznan University of Technology
Poznan, Poland

Gennadii Oborskyi
Odessa National Polytechnic University
Odessa, Ukraine

Milan Edl
University of West Bohemia
Plzeň, Czech Republic

Ivan Kuric
University of Zilina
Zilina, Slovakia

Ivan Pavlenko
Sumy State University
Sumy, Ukraine

Predrag Dasic
High Technical Mechanical School
of Professional Studies
Trstenik, Serbia

ISSN 2195-4356 ISSN 2195-4364 (electronic)
Lecture Notes in Mechanical Engineering
ISBN 978-3-030-40723-0 ISBN 978-3-030-40724-7 (eBook)
https://doi.org/10.1007/978-3-030-40724-7

This Springer imprint is published by the registered company Springer Nature Switzerland AG
The registered company address is: Gewerbestrasse 11, 6330 Cham, Switzerland

Contents

Mechanical Engineering

Mathematical Modeling of the Process of the Interaction of the Cutting Diamond Disk with the Environment

Ala Bezpalova[1], Vladimir Lebedev[2(✉)], Yuri Morozov[2], Tatiana Chumachenko[2], and Nataliya Klymenko[2]

[1] Odessa State Academy of Civil Engineering and Architecture, 4 Didriksona Street, Odessa 65029, Ukraine
[2] Odessa National Polytechnic University, 1 Shevchenko Avenue, Odessa 65044, Ukraine
wlebedev29@rambler.ru

Abstract. Cutting of solid construction materials during repair and restoration work is carried out with diamond discs and CBN discs on a metal bond with speeds up to 80 m/s. The cutting process is accompanied by significant heat generation, as a result of which the cutting disc heats up intensively. When heated to a temperature of 500–600 °C, the strength characteristics of the disk are halved, which can lead to rupture and seizure of the disk and loss of the diamond layer. Disk heating temperature should not exceed 600 °C. The operating time of the diamond cutting disc is the time during which it is heated during continuous operation to a temperature of 600 °C. The cooling media used in cutting are intensively discarded by the air flows of the boundary layer of air that circulate near the rotating circle. Knowing the speed and dimensional characteristics of these flows, we can develop a rational cooling system. The purpose of the study is to determine the conditions of transportation of cooling media, ensuring their guaranteed entry into the cutting zone to create the maximum cooling effect. This work defines the speeds of flowing air in the near-wall area and in the area tangential to the disk with the help of mathematical modeling. The thickness of the air layer, which rotates at a speed of up to 0.5 circle speed was determined, taking this value as the "boundary layer thickness". The change in air pressure in the cutting zone between the cutting grains was determined, too. It is established that air pressure can vary from 0.5–1.7 MPa. In this regard, the cooling medium supplied under the circle, inevitably displaced from the cutting zone. In order for the cooling medium to penetrate into the cutting zone, it must be fed under a pressure that exceeds the air pressure in the cutting zone.

Keywords: Boundary layer · Air pressure · Boundary layer thickness · Cutting zone · Mathematical modeling · Cooling media · Operating time · Diamond disc

1 Introduction

Cutting solid construction materials during repair and restoration work is carried out with diamond discs and CBN discs on a metal bundle, the rotation speed of which, and, consequently, the cutting speed, is 35–80 m/s. Due to the high intensity of the cutting

V. Tonkonogyi et al. (Eds.): InterPartner 2019, LNME, pp. 3–14, 2020.
https://doi.org/10.1007/978-3-030-40724-7_1

process and intensive micro-formation, the cutting process is accompanied by a significant heat release.

It should be noted that the base of the diamond discs on which the diamond abrasive coating is applied is made of ordinary low-alloyed steel, such as Steel 9HFM (0.9% carbon and up to 1% chromium, vanadium and molybdenum). These steels have a sufficiently high tensile strength to withstand high centrifugal forces, but low heat resistance. When heated to the temperature of 500–600 °C, the strength characteristics of these steels are reduced by almost 2 times, which can cause jamming or even breakage and rupture of the tool during operation.

In addition, graphitization of diamond cutting grains, that is, the conversion of tetragonal carbon to hexagonal, also occurs at a temperature of about 600 °C. Therefore, operation at this disc temperature may result in loss of the diamond layer [1, 2].

Thus, the disk heating temperature should not exceed 600 °C. Therefore, the operating time of the diamond cutting disc is the time during which it is heated during continuous operation to a temperature of 600 °C. The longer this time, the higher the resistance of the diamond disc.

Mathematical modeling was carried out in [1], which allows determining the time of safe operation up to a critical temperature taking into account the features of heat exchange between a cutting metal disk and the environment.

This time could be increased by cooling the cutting zone; however, in practice, very often cooling fluids are intensively discarded by air streams that circulate near the rotating wheel. Knowing the speed and dimensional characteristics of these flows, we can develop a rational cooling system.

2 Literature Review

Despite the significant amount of works, there is no description of the case that arises during the rotation of the cutting diamond disk. The works fall into two groups, experimental and theoretical. However, as a rule, studies are carried out for very large Reynolds numbers (of the order of 2,000,000 and higher), while in our case the largest value of Reynolds numbers is, respectively, for angular velocities:

$$\Omega_D = 30\,m/s \rightarrow Re = 190.5001905$$
$$\Omega_D = 50\,m/s \rightarrow Re = 245.9346884$$
$$\Omega_D = 80\,m/s \rightarrow Re = 311.0855085$$

In addition, experimental data require generalizations, which also require a large amount of experimental work.

In [3], the boundary layer near a rotating disk is considered, but the work is based on experiment. In addition, measurements do not take into account the nature of the disk surface, which makes the model more preferable.

In [4], a mathematical simulation of air flow around a rotating disk was performed. However, conditions for very large Reynolds numbers are considered and it is impossible to attach results to our case.

In [5], the case of a rotating disk in a liquid with very large Reynolds numbers is considered. The results of this study cannot be used for our case, since the movement in a liquid is considered.

In [6], the boundary layer of air near a rotating disk is investigated. The work is experimental. It is difficult to relate to the process under study since generalizations are needed for small Reynolds numbers.

In [7], a turbulent boundary layer near a rotating disk is considered. Studies are conducted for very large Reynolds numbers. The results do not correlate with the case under study.

An experimental study of changes in the boundary layer of a rotating disk was performed in [8]. This is experimental work. The obtained patterns are difficult to generalize for other cases.

In [9, 10], the boundary layer near the rotating disk is investigated. This is experimental work. The obtained patterns are difficult to generalize for other cases.

3 Research Methodology

The purpose of this work is to determine the conditions of transportation of cooling media, ensuring their guaranteed entry into the cutting zone to create the maximum cooling effect using the patterns of interaction of the cutting wheel with the ambient air.

The tasks solved in this paper are as follows:

1. Mathematical modeling in order to determine the patterns of change in the velocity of flowing air in the near-wall area and in the area tangential to the disk.
2. Mathematical modeling to determine the thickness of the air layer, which rotates at a speed of up to 0.5 circle speed, taking this value as the “boundary layer thickness”.
3. Mathematical modeling in order to determine the change in air pressure in the cutting zone between cutting grains because of heating and some compression during the cutting process.

Calculations are carried out in accordance with the scheme of Fig. 1 [11, 12].

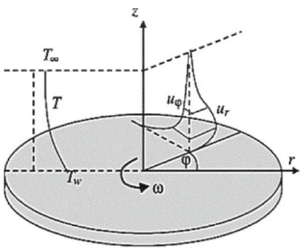

Fig. 1. Design scheme.

For this scheme, the Navier-Stokes equation in the moving coordinate system will be:

$$\frac{\partial u_\rho}{d\rho} + \frac{u_\rho}{\rho} + \frac{1}{\rho}\frac{\partial \upsilon_\varphi}{\partial \varphi} + \frac{\partial w}{\partial z} = 0 \tag{1}$$

$$\frac{\partial u_\rho}{\partial t} + (\mathbf{u}\cdot\nabla)u_\rho - \frac{\upsilon_\varphi^2}{\rho} - 2\upsilon_\varphi\Omega_D = -\frac{1}{\rho_*}\frac{\partial p}{\partial \rho} + v[\nabla^2 u_\rho - \frac{u_\rho^2}{\rho^2} - \frac{2}{\rho^2}\frac{\partial \upsilon_\varphi}{\partial \varphi}] \tag{2}$$

$$\frac{\partial \upsilon_\varphi}{\partial t} + (\mathbf{u}\cdot\nabla)\upsilon_\varphi + \frac{u_\rho \upsilon_\varphi}{\rho} + 2u_\rho\Omega_D = -\frac{1}{\rho\rho_*}\frac{\partial p}{\partial \varphi} + v[\nabla^2 \upsilon_\varphi + \frac{2}{\rho^2}\frac{\partial u_\rho}{\partial \varphi} - \frac{\upsilon_\varphi}{\rho^2}] \tag{3}$$

$$\frac{\partial w}{\partial t} + (\mathbf{u}\cdot\nabla)w = -\frac{1}{\rho_*}\frac{\partial p}{\partial z} + v\nabla^2 w \tag{4}$$

where, $v-$ kinematic viscosity coefficient; ρ_*- air density; $p-$ excess pressure in the boundary layer; Ω_D- disk angular velocity; ∇ и ∇^2 gradient and Laplace operator in a cylindrical coordinate system (ρ, φ, z).

Instant radial, azimuth and axial speeds $\{u_\rho, \upsilon_\varphi, w\}$ and instant pressure p can be decomposed into averaged (time independent) and fluctuation (time dependent) components, i.e., Reynolds decomposition.

$$\begin{aligned}&\tilde{u}_\rho = U^*(z) + u_\rho^*(t,\rho,\varphi,z), \tilde{\upsilon}_\varphi = V^*(z) + \upsilon_\varphi^*(t,\rho,\varphi,z),\\ &\tilde{w} = W^*(z) + w^*(t,\rho,\varphi,z)\end{aligned} \tag{5}$$

Based on the theory of the boundary layer and taking the axial symmetry (we exclude all derivatives with respect to the variable φ), and also taking into account the linearity of the solution of system (1)–(4) taking into account decomposition (5), we write the system of equations for $\{U^*(z), V^*(z), W^*(z)\}$:

$$\frac{\partial U^*}{d\rho} + \frac{U^*}{\rho} + \frac{\partial W^*}{\partial z} = 0 \tag{6}$$

$$U^*\frac{\partial U^*}{\partial \rho} + W^*\frac{\partial U^*}{\partial z} - \frac{V^{*2}}{\rho} - 2V^*\Omega_D = -\frac{1}{\rho_*}\frac{\partial p}{\partial \rho} + v\left(\frac{\partial^2 U^*}{\partial \rho^2} + \frac{\partial}{\partial \rho}\left(\frac{U^*}{\rho}\right) + \frac{\partial^2 U^*}{\partial z^2}\right) \tag{7}$$

$$U^*\frac{\partial V^*}{\partial \rho} + W^*\frac{\partial V^*}{\partial z} + \frac{U^* V^*}{\rho} + 2U^*\Omega_D = v\left(\frac{\partial^2 V^*}{\partial \rho^2} + \frac{\partial}{\partial \rho}\left(\frac{V^*}{\rho}\right) + \frac{\partial^2 V^*}{\partial z^2}\right) \tag{8}$$

$$U^*\frac{\partial W^*}{\partial \rho} + W^*\frac{\partial W^*}{\partial z} = -\frac{1}{\rho_*}\frac{\partial p}{\partial z} + v\left(\frac{\partial^2 W^*}{\partial \rho^2} + \frac{W^*}{\rho} + \frac{\partial^2 W^*}{\partial z^2}\right) \tag{9}$$

We introduce new functions moving to the dimensionless form

$$U(z) = \frac{U^*}{\rho\Omega Ro}, V(z) = \frac{V^*}{\rho\Omega Ro}, W(z) = \frac{W^*}{L\Omega Ro}, P(\rho, z) = \frac{p}{\rho_* L^2 \nu \Omega^2 Ro^2} \quad (10)$$

and for vertical and radial directions $\xi = z/L, L = (\nu/\Omega)^{1/2}, r = \rho/L$

We obtain the following system of differential equations:

Options Ro and $Co = 2 - Ro - Ro^2$ were studied in [12].

Bödewadt flow:	$Ro = 1$	$Co = 0$	$\Omega = \Omega_F$
Ekman flow:	$Ro = 0$	$Co = 2$	$\Omega = \Omega_F = \Omega_D$
Von Kármán:	$Ro = -1$	$Co = 2$	$\Omega = \Omega_D$

The boundary conditions are written as follows:

$$U(0) = \lambda U'(0),\ V(0) = \eta V'(0),\ W(0) = 0;\ \lim_{z \to \infty} \{U(z), V(z)\} = \{0, 1\}$$

where, $\lambda, \eta -$ experimental coefficients of the surface roughness of the circle in the radial and angular directions, respectively.

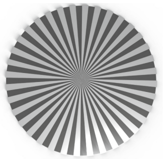

Fig. 2. Radial grooves.

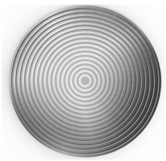

Fig. 3. Concentric grooves.

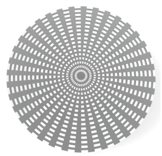

Fig. 4. Isotropic roughness.

The boundary conditions for a smooth disk are set at $\lambda = \eta = 0$. Special cases $\eta > 0, \lambda = 0 -$ (concentric grooves, Fig. 3) and $\eta = 0, \lambda > 0 -$ (radial grooves Fig. 2) correspond to anisotropic roughness of the radial and azimuth, the case when $\lambda = \eta \neq 0 -$ corresponds to isotropic roughness Fig. 4. Initial values for $U'(0)$и $V'(0)$ for different roughness parameters λ and η when $Ro = -1$и $Co = 2$ presented in the tables of sources [1, 2].

Introducing new functions,

$\phi_1(z) = U(z),\ \phi_2(z) = U'(z),\ \phi_3(z) = V(z),\ \phi_4(z) = V'(z),\ \phi_5(z) = W(z)$, transform the system of Eqs. (6)–(10) into the corresponding system the first order differential equations:

$$\begin{gathered} \phi_1'(z) = \phi_2(z),\ \phi_2'(z) = Ro\big(\phi_1^2(z) + \phi_5(z)\phi_2(z) - (\phi_3^2(z) - 1)\big) - Co(\phi_3(z) - 1) \\ \phi_3'(z) = \phi_4(z),\ \phi_4'(z) = Ro(2\phi_1(z)\phi_3(z) + \phi_4(z)\phi_5(z)) + Co\phi_1(z),\ \phi_5'(z) = -2\phi_1(z) \end{gathered} \quad (11)$$

$$\phi_1(0) = \lambda\phi_1'(0),\ \phi_3(0) = \eta\phi_4(0),\ \phi_5(0) = 0;\ \lim_{z \to \infty} \{\phi_1(z), \phi_3(z)\} = \{0, 1\} \quad (12)$$

Figures 5*a*, *b*, *c* present studies of the dependence of the averaged radial *U(z)*, tangential *V(z)* and axial *W(z)* components of the velocity field of the roughness parameters. Considered cases of radial $\eta > 0, \lambda = 0$ (Fig. 5*a*) and isotropic roughness $\lambda = \eta \neq 0$ (Fig. 5*b, c*).

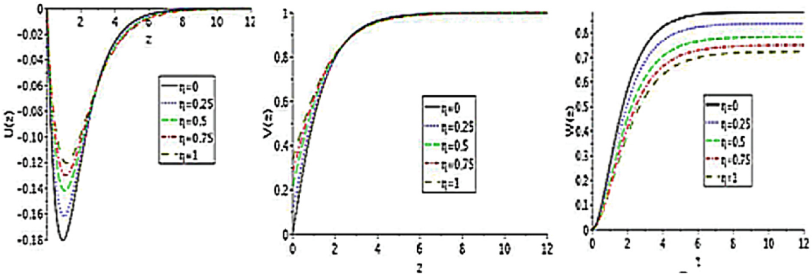

Fig. 5. Dependencies in dimensionless form of averaged radial U(z), tangential V(z) and axial W(z) components of the velocity field of the roughness parameters. a – radial roughness, b, c – isotropic roughness.

Based on the theory of the boundary layer and taking the axial symmetry (excluding all derivatives with respect to the variable φ), as well as considering the temperature, relatively $\{u^*_\rho, \upsilon^*_\varphi, w^*\}$ we can write the following dynamic system of equations:

$$\frac{\partial u^*_\rho}{d\rho} + \frac{u^*_\rho}{\rho} + \frac{\partial w^*}{\partial z} = 0 \tag{13}$$

$$\frac{\partial u^*_\rho}{\partial t} + u^*_\rho \frac{\partial u^*_\rho}{\partial \rho} - \frac{\upsilon^{*2}_\varphi}{\rho} + w^* \frac{\partial w^*}{\partial z} = -\frac{1}{\rho_*}\frac{\partial p}{\partial \rho} + v[\frac{\partial^2 u^*_\rho}{\partial \rho^2} + \frac{\partial}{\partial \rho}(\frac{u^*_\rho}{\rho}) + \frac{\partial^2 u^*_\rho}{\partial z^2}] \tag{14}$$

$$\frac{\partial \upsilon^*_\varphi}{\partial t} + u^*_\rho \frac{\partial \upsilon^*_\varphi}{\partial \rho} + \frac{u_\rho \upsilon^*_\varphi}{\rho} + w \frac{\partial \upsilon^*_\varphi}{\partial z} = v[\frac{\partial^2 \upsilon^*_\varphi}{\partial \rho^2} + \frac{\partial}{\partial \rho}(\frac{\upsilon^*_\varphi}{\rho}) + \frac{\partial^2 \upsilon^*_\varphi}{\partial z^2}] \tag{15}$$

$$\frac{\partial w^*}{\partial t} + u^*_\rho \frac{\partial w^*}{\partial \rho} + w^* \frac{\partial w^*}{\partial z} = -\frac{1}{\rho_*}\frac{\partial p}{\partial z} + v[\frac{\partial^2 w^*}{\partial \rho^2} + \frac{1}{\rho}\frac{\partial w^*}{\partial \rho} + \frac{\partial^2 w^*}{\partial z^2}] \tag{16}$$

$$\rho_* C_p\left(\frac{\partial T}{\partial t} + u^* \frac{\partial T}{\partial \rho} + w^* \frac{\partial T}{\partial z}\right) = k\left(\frac{\partial^2 T}{\partial \rho^2} + \frac{1}{\rho}\frac{\partial T}{\partial \rho} + \frac{\partial^2 T}{\partial z^2}\right) \tag{17}$$

where $C_p -$ specific heat; $k -$ coefficient of thermal conductivity.

The boundary conditions for speeds and temperatures are

$$\left.\begin{array}{l} u^*(t,\rho,z)|_{z=0}=0, \upsilon^*_\varphi(t,\rho,z)\Big|_{z=0}=\rho\Omega_0(1-\alpha t)^{-1}, w^*(t,\rho,z)|_{z=0}=0, T(t,\rho,z)|_{z=0}=T_D \\ u^*(t,\rho,z)=0, \upsilon^*_\varphi(t,\rho,z)=0, p(t,\rho,z)=0, T=T_\infty \; npu \; z\to 0 \end{array}\right\}$$

where $\Omega_0(1-\alpha t)^{-1}-$ disk angular velocity; $\alpha-$ determines the rate of change of the angular velocity of the disk; T_D- disk temperature $\alpha-$ disk acceleration.

Using the transformations proposed in [1, 2] we have:

$$\begin{array}{l} u^*(t,\rho,z)=\rho\Omega_0(1-\alpha t)^{-1}F(\eta), \upsilon^*_\varphi(t,\rho,z)=\rho\Omega_0(1-\alpha t)^{-1}G(\eta) \\ w^*(t,\rho,z)=-2\sqrt{v\Omega_0}(1-\alpha t)^{-1/2}H(\eta), p(t,\rho,z)=-\rho v\Omega_0(1-\alpha t)^{-1}P(\eta) \\ T(t,\rho,z)=T_\infty+(T_d-T_\infty)\Theta(\eta) \end{array} \quad (18)$$

Where $\eta=z\sqrt{\Omega_0/v}(1-\alpha t)^{-1/2}-$ new variable.

Instead of system (13)–(17), we obtain the following system of differential equations for new functions:

$$H'(\eta)-F(\eta)=0 \quad (19)$$

$$F''(\eta)+2H(\eta)F'(\eta)-F^2(\eta)+G^2(\eta)-\tilde{\alpha}(F(\eta)+\eta 2^{-1}F'(\eta))=0 \quad (20)$$

$$G'(\eta)+2H(\eta)G'(\eta)-2F(\eta)G(\eta)-\tilde{\alpha}(G(\eta)+\eta 2^{-1}G'(\eta))=0 \quad (21)$$

$$P'(\eta)-4H(\eta)F(\eta)-2F'(\eta)+\tilde{\alpha}(H(\eta)+\eta F(\eta))=0 \quad (22)$$

$$\Theta''(\eta)+2P_rH(\eta)\Theta'(\eta)-\frac{\eta}{2}\tilde{\alpha}P_r\Theta(\eta)=0 \quad (23)$$

where $\tilde{\alpha}=\alpha/\Omega_0-$ dimensionless parameter; $P_r=C_p\mu/k-$ Prandtl number.

The corresponding boundary conditions for the velocity and temperature fields (23) transform into:

$$\left.\begin{array}{l} F(\eta)|_{\eta=0}=0, G(\eta)|_{\eta=0}=1, H(\eta)|_{\eta=0}=0, \Theta(\eta)|_{\eta=0}=1, \\ F(\eta)=0, G(\eta)=0, P(\eta)=1, \Theta(\eta)=0 \; npu \; \eta\to 0 \end{array}\right\} \quad (24)$$

Introducing new functions,

$$\begin{array}{l} \phi_1(\eta)=F(\eta),\ \phi_2(\eta)=F'(\eta),\ \phi_3(\eta)=G(\eta),\ \phi_4(\eta)=G\prime(\eta), \\ \phi_5(\eta)=H(\eta),\ \phi_6(\eta)=\Theta(\eta),\ \phi_8(\eta)=\Theta'(\eta), \end{array}$$

transform the system of Eqs. (19)–(23) into the corresponding system of differential equations of the first order:

$$\begin{aligned}&\phi_1'(\eta) = \phi_2(\eta),\ \phi_2'(\eta) = \phi_1^2(\eta) - \phi_3^2(\eta) - 2\phi_2(\eta)\phi_5(\eta) + \tilde{\alpha}(\phi_1(\eta) + \eta 2^{-1}\phi_2(\eta))\\&\phi_3'(\eta) = \phi_4(\eta),\ \phi_4'(\eta) = 2\phi_1(\eta)\phi_3(\eta) - \phi_4(\eta)\phi_5(\eta) + \tilde{\alpha}(\phi_3(\eta) + \eta 2^{-1}\phi_4(\eta))\\&\phi_5'(\eta) = \phi_1(\eta),\ \phi_6'(\eta) = 4\phi_1(\eta)\phi_5(\eta) + 2\phi_2(\eta)\end{aligned} \tag{25}$$

$$\left.\begin{aligned}&\phi_1(\eta)|_{\eta=0} = 0, \phi_3(\eta)|_{\eta=0} = 1, \phi_5(\eta)|_{\eta=0} = 0\phi_6(\eta)|_{\eta=0} = 1,\\&\phi_1(\eta) = 0, \phi_3(\eta) = 0, \phi_6(\eta) = 0\ npu\ \eta \to 0\end{aligned}\right\} \tag{26}$$

Initial values for *F'(0)*, *G'(0)* and *H(∞)* for various parameters $\tilde{\alpha}$ are shown in Table 4 [12].

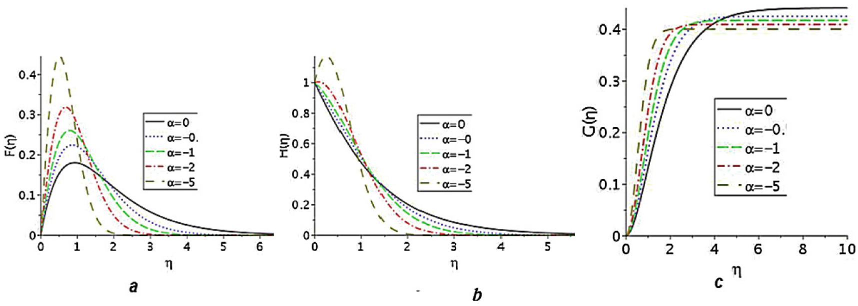

Fig. 6. The results of numerical studies of the dependence in dimensionless form of the radial *F (η)*, tangential *G(η)* and axial *H(η)* velocity field components for various parameter values $\tilde{\alpha}$. a, b graphs are given for a fixed value of the Prandtl number - and various values of the dimensionless parameter $\tilde{\alpha}$, 6 b with fixed parameter $\tilde{\alpha} = -1$ and different values of the Prandtl number.

The results of numerical studies of the dependence of the radial *F(η)*, tangential *G (η)* and axial *H(η)* velocity field components for various parameter values $\tilde{\alpha}$ are presented in Fig. 6a, b, c. From the above figures it can be seen: the change in the radial component *F(η)* (Fig. 6*a*) indicates that the boundary layer becomes thinner and more pronounced with increasing $\tilde{\alpha}$; the boundary layer becomes thinner *G(η)* (Fig. 6*b*), it shows that the speed of rotation of the boundary layer is less than the speed of the disk at small values of the parameter $\tilde{\alpha}$; characteristic decrease in the thickness of the boundary layer with increasing $\tilde{\alpha}$ can be seen on the graph for the axial component *H(η)* (Fig. 6*c*).

The expression for estimating the thickness of the boundary layer is:

$$\delta_T = \eta_\delta \sqrt{v/\Omega_0}(1 - \alpha t)^{1/2} = \eta_\delta \sqrt{v/\Omega(t)} \tag{27}$$

Where, η_δ measure of the dimensionless thickness of the thermal boundary layer, defined as the value η, at which the dimensionless temperature has dropped to one percent of its value on the disk, i.e. $\Theta(\eta_\delta) = 0.01$.

To go from dimensionless to dimensional values, it is necessary to solve Eq. 24 with respect to Ω_0.

It can be argued that near the cutting wheel there is always a boundary layer of air 2–3 mm thick rotating with it (if we assume the thickness of the boundary layer to a speed of 0.5 disk speed), which penetrates into the zone of contact of the cutting circle with the part. The interaction of this air with the components of the cutting zone is discussed below (Fig. 7).

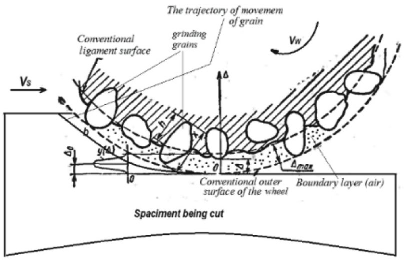

Fig. 7. Vw-speed of the circle, Vs-speed of the sample.

The interaction of air with the wheel and with the detail in the contact zone can be considered on the basis of the following considerations.

If we consider the space enclosed between the conditional outer surface and the conditional surface of the ligament, then we can see that this space is filled with grains protruding from the ligament, between which there is air. Thus, between the grains, the grinding wheel and its conventional surfaces there are some amounts of air. During the cutting of material around, the grains of the latter will partially go deep into the material, and partly into the bundle. This will lead to the fact that the distance between the conditioned surfaces will decrease, and, consequently, the volume of air will also decrease, i.e. the air will shrink.

In addition, when cutting metal grains of a circle, a high temperature occurs, a large heat release occurs, as a result of which the temperature of the air enclosed between the grains of the circle should increase.

Thus, when grinding, the air that has penetrated into the zone of contact of the wheel with the part is subjected to simultaneous compression and heating, and therefore the Clayperon equation can be applied in the first approximation. In accordance with this equation, the air pressure will be:

$$Pair = RT/V \tag{28}$$

where, R - universal gas constant; V - the volume of air in the zone of contact of the circle with the sample between the grains, the bundle and the workpiece; T - temperature in °K in the contact zone.

The increase in pressure due to compression and increase in air temperature can be calculated by the expression

$$P_{air} = \frac{\left(T_{gr} + 273\right)\Delta}{293(\Delta - f - f_1)} \times 0,1\,\mathrm{MPa} \quad (29)$$

where, Tgr - grain cutting temperature Δ - the center of the distribution curve grouping describing the removal of the vertices of the grains from the conditional surface of the ligament, f, f_1 - the deepening of grain in the bundle and in the material under the action of force $P_{y.}$

All these values are taken by source [13]. The results of the calculation of air pressure in the zone of contact of the circle with the part are shown in Fig. 8.

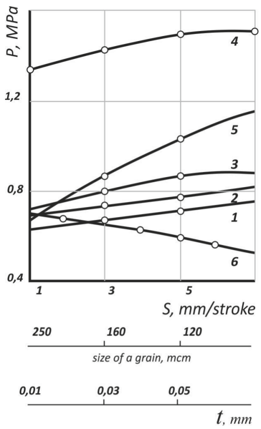

Fig. 8. The calculated dependences of the air pressure in the zone of contact of the cutting wheel with the part. 1, 2, 3-curves for grains 25, 16, 12. Curve 4 - P_{air} air pressure dependence on wheel speed f(Vw), 5 - P_{air} - air pressure dependence on speed of specimen f(Vsp). 6 - P_{air} - air pressure dependence on size of grain. Mode of grinding- V_{sp} speed of specimen = 0.15 m/s; V_w speed of wheel = 30 m/s; S cross feed = 2 mm per stroke. Material – ZrO_2 HRC = 62, machine-tool 3G71.

4 Results

As a result of the research conducted, it has been established that around a rotating cutting wheel there is always a boundary layer of air 2–3 mm thick, regardless of the roughness of the circle surfaces.

The air flow of the boundary layer discards cooling media from the cutting zone.

In addition, despite the fact that the speed of the air flow is somewhat less than the speed of rotation of the circle, this layer penetrates into the zone of contact of the circle with the part where it undergoes some compression and considerable heating.

As a result, the air pressure in the zone of contact of the circle with the part increases to 0.5–1.5 MPa. This prevents the penetration of cooling media into the cutting area, so cutting is almost always carried out "dry".

5 Conclusions

Mathematical modeling in order to determine the patterns of change in the velocities of the flowing air in the near-wall region and in the area tangential to the disc made it possible to determine these values for specific cutting conditions of stone materials.

Mathematical modeling to determine the thickness of the air layer, which rotates at a speed of up to 0.5-wheel speed, taking this value as the "thickness of the boundary layer" made it possible to determine the thickness of the air boundary layer near the rotating cutting wheel, determine the velocity distribution over the thickness of this layer and prove that the air is always in the contact zone of the circle and the part.

Mathematical modeling to determine the change in air pressure in the cutting zone between cutting grains during heating and some compression during the cutting process made it possible to determine that air pressure can vary from 0.5 to 1.5 MPa. In this regard, the cooling medium supplied under the circle, inevitably displaced from the cutting zone.

In order for the cooling medium to penetrate the cutting zone, it must be fed under a pressure that exceeds the air pressure in the cutting zone.

References

1. Lebedev, V., Bezpalova, A., Tonkonogyi, V., Morozov, Y., Frolenkova, O.: Cutting stone building materials and ceramic tiles with diamond disc. In: Proceedings of the International Conference on Design, Simulation, Manufacturing: The Innovation Exchange, DSMIE-2019, 11–14 June, Lutsk, Ukraine, pp. 180–187 (2019)
2. Lebedev, V., Frolenkova, O., Chumachenko, T., Bespalova, A.: Predel'noye vremya raboty almaznogo diska pri razrezanii kamennykh materialov. In: Materialy 19-go Mezhdunar. nauch.-tekhn. seminara, 18–22 fevralya 2019, pp. 109–112. Koshitse-Kiyev, ATM Ukrainy (2019)
3. Shintaro Imayama, R.J., Lingwood, P., Alfredsson, H.: The turbulent rotating-disk boundary layer. Eur. J. Mech.-B/Fluids **48**, 245–253 (2014)
4. Appelquist, E., Schlatter, P., Alfredsson, P., Lingwood, R.: Turbulence in the rotating-disk boundary layer investigated through direct numerical simulations. Eur. J. Mech.-B/Fluids **70**, 6–18 (2018)
5. Cebeci, T., Abbott, D.E.: Boundary layers on a rotating disk. AIAA J. **1**(6), 561–567 (1975)
6. Imayama, S.: Experimental study of the rotating-disk boundary-layer flow. Technical reports from Royal Institute of Technology KTH Mechanics SE-100 44, Stockholm, Sweden (2012)
7. Parthasarathy, R.: Analysis of the turbulent boundary layer on a rotating disk. Microsyst. Technol. **8**(4–5), 278–281 (2002)
8. Kohama, Y.: Study on boundary layer transition of a rotating disk. Acta Mech. **50**(3–4), 193–199 (1984)
9. Imayama, S.: Studies of the rotating-disk boundary-layer flow. Technical reports from Royal Institute of Technology KTH Mechanics SE-100 44, Stockholm, December 2014
10. Cham, T., Head, M.: Turbulent boundary-layer flow on a rotating disk. J. Fluid Mech. **37**(1), 129–147 (1969)
11. Lingwood, R., Garrett, S.: The effects of surface mass flux on the instability of the BEK system of rotating boundary-layer flows. Eur. J. Mech.-B/Fluids **30**(3), 299–310 (2011)

12. Watson, L., Wang, C.: Deceleration of a rotating disk in a viscous fluid. Phys. Fluids **22**, 2267–2269 (1979)
13. Reznikov, A.N.: Abrazivnaya i almaznaya obrabotka materialov. Mashinostroyeniye, Moscow (2013)